

Forebody asymmetric vortex control with extended dielectric barrier discharge plasma actuators

Borui Zheng(郑博睿), Ming Xue(薛明), Chang Ge(葛畅)

Citation: Chin. Phys. B . 2020, 29(6): 064703 . **doi:** 10.1088/1674-1056/ab8372
Journal homepage: http://cpb.iphy.ac.cn; http://iopscience.iop.org/cpb

What follows is a list of articles you may be interested in

Dynamic evolution of vortex structures induced bytri-electrode plasma actuator

Bo-Rui Zheng(郑博睿), Ming Xue(薛明), Chang Ge(葛畅)

Chin. Phys. B . 2020, 29(2): 024704 . **doi:** 10.1088/1674-1056/ab671f

Enhancement of corona discharge induced wind generation with carbon nanotube and titanium dioxide decoration

Jianchun Ye(叶建春), Jun Li(李俊), Xiaohong Chen(陈晓红), Sumei Huang(黄素梅), Wei Ou-Yang(欧阳威)

Chin. Phys. B . 2019, 28(9): 095202 . **doi:** 10.1088/1674-1056/ab33ed

Electrical and thermal characterization of near-surface electrical discharge plasma actuation driven by radio frequency voltage at low pressure

Zhen Yang(杨臻), Hui-Min Song(宋慧敏), Di Jin(金迪), Min Jia(贾敏), Kang Wang(王康)

Chin. Phys. B . 2018, 27(8): 085205 . **doi:** 10.1088/1674-1056/27/8/085205

Comparison between AlN and Al_2O_3 ceramics applied to barrier dielectric of plasma actuator

Dong-Liang Bian(卞栋梁), Yun Wu(吴云), Min Jia(贾敏), Chang-Bai Long(龙昌柏), Sheng-Bo Jiao(焦胜博)

Chin. Phys. B . 2017, 26(8): 084703 . **doi:** 10.1088/1674-1056/26/8/084703

Wind tunnel experiments on flow separation control of an Unmanned Air Vehicle by nanosecond discharge plasma aerodynamic actuation

Kang Chen(陈康) and Hua Liang(梁华)

Chin. Phys. B . 2016, 25(2): 024703 . **doi:** 10.1088/1674-1056/25/2/024703

Forebody asymmetric vortex control with extended dielectric barrier discharge plasma actuators*

Borui Zheng(郑博睿)[1,†], Ming Xue(薛明)[2], and Chang Ge(葛畅)[1]

[1] School of Automation and Information Engineering, Xi'an University of Technology, Xi'an 710048, China
[2] School of Aeronautics, Northwestern Polytechnical University, Xi'an 710072, China

(Received 27 January 2020; revised manuscript received 27 February 2020; accepted manuscript online 26 March 2020)

Plasma control of forebody asymmetric vortices is mostly achieved by means of dielectric barrier discharge (DBD) plasma actuators. However, DBD actuators suffer from some disadvantages such as a weak induced body force, a single-direction induced jet, and an unclear control mechanism. We carry out wind tunnel experiments involving the forebody vortex control of a slender body at high angles of attack using an innovative extended DBD actuator, which has a stronger capacity to induce an electric wind than a DBD actuator. Through synchronous measurements of the pressure distribution and particle image velocimetry (PIV), the spatiotemporal evolution of the dynamic interactions between plasma-actuation-induced vortices and forebody asymmetric vortices is analyzed. The influence of plasma discharge on the boundary layer separation around a slender body and the spatial topological structures of asymmetric vortices are further surveyed, as the optimized actuation parameters. Extended DBD actuators are found to be more capable of controlling asymmetric vortices than DBD actuators, and a linear proportionality of the sectional lateral force versus the duty ratio is achieved. There exists an optimal normalized reduced frequency ($f^+ = 2\pi f_p d/U_\infty = 2.39$) for asymmetric vortex control under the present experimental conditions. The research results can provide technical guidance for the control and reuse of forebody asymmetric vortices.

Keywords: plasma flow control, dielectric barrier discharge, forebody asymmetric vortex

PACS: 47.32.Ff, 47.85.Gj, 52.80.−s **DOI:** 10.1088/1674-1056/ab8372

1. Introduction

To gain tactical advantages, advanced fighter aircrafts around the world are often required to design with higher maneuverability and agility. The improvement of the maneuverability and agility of an fighter aircraft mainly depends on the improvement of its flight performance at high angles of attack.[1] When a slender body aircraft is at high angles of attack, lateral forces in random directions and with variable magnitudes will be produced, even if the sideslip angle is zero. Under these conditions, the vertical tail, horizontal tail and rudder control surface of the aircraft all lie in the vortex wake of the wings and fuselage, resulting in a serious deficiency in the lateral-directional controllability.[2] The direct causes of these random lateral forces are the forebody asymmetric vortices that form in the leeward region of the slender fuselage of the aircraft. The directions and magnitudes of these lateral forces are determined by these forebody asymmetric vortices, which have different intensities and positions.[3,4] Meanwhile, the forebody of the fuselage is still subjected to an undisturbed airflow, and the flow around a slender body at high angles of attack is very sensitive to microdisturbances (such as turbulence, surface roughness, and slight geometric tolerances) near the tip of the slender forebody model. Therefore, the purpose of forebody vortex control is to systematically manipulate the forebody flow by inhibiting the formation and development of asymmetric vortices to provide controlled yawing moments at angles of attack at which the effectiveness of a conventional rudder decreases. By modulating the vorticity intensity and spatial positions of the asymmetric vortices at the tip of the slender body, the aerodynamic control efficiency at high angles of attack is enhanced, and the asymmetry flow problem of the separation vortices at the tip of the slender body is solved. In addition, proportional control of the random lateral forces and moments can also be realized in this way.

Generally, forebody vortex control technology can be divided into passive control technology and active control technology based on whether there is any external energy input. Passive control technology is simple in structure and does not require an energy input. Generally, only a few limited states can be effectively controlled with such technology. Under other conditions, the control efficiency may be reduced, or control efforts may even yield an effect that is opposite to the desired effect, and it can be difficult to achieve proportional control of the lateral forces and moments. This situation is not conducive to practical applications in the intelligent flight of advanced aircraft. The various available passive control technologies include bumps, dimples, strakes, fluttering

*Project supported by the National Natural Science Foundation of China (Grant Nos. 51607188 and 61971345), the Foundation for Key Laboratories of National Defense Science and Technology, China (Grant No. 614220202011801), the Natural Science Basic Research Program of Shaanxi Province of China (Grant No. 2019JM-393), and Xi'an Municipal Science and Technology Project of China (Grant No. 201805037YD15CG21(28)).

†Corresponding author. E-mail: narcker@xaut.edu.cn

© 2020 Chinese Physical Society and IOP Publishing Ltd

flags, vortex generators, nose bluntness devices, and boundary layer transition strips.[1] In all the cases, the goal is to eliminate lateral forces by changing the distribution of the forebody vortices. Thus, passive flow control methods cannot take advantage of the forebody vortex asymmetry to enhance aircraft maneuverability.

As an alternative approach, extensive investigations have focused on active control technology, which requires a continuous input of energy and can be utilized for the adaptive control of various states in real time. However, most active control systems have a relatively complex structure, and their power consumption and weight are major contributors to their associated costs or penalties. Specifically, active control technologies include vortex generators, microblowers, synthetic jets, plasma actuators, nose axial blowers, and microballoon strakes.[5] Currently, simultaneous closed-loop control and linear proportional control of lateral forces can already be achieved through plasma actuation.[6] Therefore, increasing attention has focused on forebody vortex control via plasma actuation.

In recent years, researchers in various countries have conducted numerous studies involving the plasma control of the forebody asymmetric vortices that form near slender bodies at high angles of attack, mainly focusing on answering the following three questions: (1) How can the control efficiency of a plasma actuator itself be improved? Generally, the effectiveness of the control of asymmetric vortices can be improved by optimizing the electrical parameters and geometric configuration of the plasma actuator or by changing the discharge regime of the plasma actuation by using proper power supplies. (2) How can the gap with respect to actual engineering applications be narrowed? Related studies have focused on expanding the ranges of wind speed and angle of attack in which effective control can be achieved through plasma actuation, realizing linear proportional control and closed-loop control of lateral forces, and deriving universally control laws relevant to actual engineering applications. (3) What is the fundamental control mechanism of plasma actuation for forebody asymmetric vortices? The purpose is to understand the spatiotemporal evolution of the dynamic interactions between plasma-actuation-induced vortices and forebody asymmetric vortices, which is a basic requirement to control and facilitate the lateral forces effectively.

At present, particle image velocimetry (PIV) flow field visualization technique is commonly adopted to obtain high-resolution images of the spatiotemporal evolution of the dynamic interactions between plasma-induced and asymmetric vortices. In the future, it will be necessary to combine computational fluid dynamics methods with wind tunnel experiments to better understand the control mechanisms of plasma actuation acting on the boundary layer separation of the flow field around slender bodies and the spatial topological structures of the asymmetric vortices.

To solve the first problem and to improve the performance of plasma actuators, Maslov *et al.*[7] proposed the use of an arc discharge to change the separation positions of the boundary layer on both sides of a slender body and to suppress the asymmetric characteristics of the vortex pair with respect to the slender body. However, because arc discharge is unstable and occurs at high temperatures, it is easy to burn through the electrode. Therefore, dielectric barrier discharge (DBD) was adopted in most subsequent studies. Wang *et al.*[8] improved the control efficiency of a DBD plasma actuator by optimizing its configuration and installation position. Zheng *et al.*[9] proposed a double-sided sliding discharge plasma actuator and, by comparing the results of wind tunnel experiments for three different methods of applying plasma actuation to forebody vortices, found that extended DBD (EX-DBD) actuation yielded a better control effect than other plasma actuation methods. However, the interactions between plasma-actuation-induced and asymmetric vortices have not been analyzed.

There are three main ways to narrow the gap with actual engineering applications: (1) The first is to broaden the controllable ranges of wind speeds and angles of attack. Zheng *et al.*[10] used a peristaltic acceleration pulsed power supply to improve the effective wind speed and angle of attack ranges (25 m/s and 50°) for forebody vortex control with DBD actuation. By using nanosecond pulsed plasma discharge, Long *et al.*[11] achieved effective control of the asymmetric flow field around a slender body at wind speeds up to 42 m/s and angles of attack up to 55°. (2) The second way to narrow the gap is through linearly proportional control. Linearly proportional control of the lateral force and moment of a slender body at high angles of attack can be achieved by changing the pulsed duty ratio of singled-side plasma actuation or adopting a double-sided duty cycle modulation technique.[12,13,15] (3) The third way to narrow the gap is through closed-loop control. Among the active flow control technologies that are currently available, plasma actuators can already be employed to achieve the closed-loop control and proportional control of lateral forces.[6,11–14] In conclusion, with respect to narrowing the gap with actual engineering applications, the experimental results show that proportional control of the lateral force and moment of a slender body at high angles of attack can be achieved by means of pulsed plasma actuation, but the controllable ranges are still far from those required in actual applications. In the future, research will focus on establishing more effective plasma actuator and discharge regimes to improve the control efficiency and on gaining a better understanding of the fundamental control mechanism for asymmetric vortices in targeted flow control scenarios.

To investigate the control mechanism of plasma actuation for forebody asymmetric vortices and to understand the interactions between the asymmetric vortices and the vortices induced by plasma actuation, some scholars have applied pulsed plasma discharge to change the positions of the separation points by creating unequal boundary layer momentums on both sides of the apex of the slender model, thereby affecting the spatial distribution of the asymmetric vortices. By adjusting the duty ratio of the pulsed plasma discharge, proportional control of the spatial distribution of the asymmetric vortex in the leeward region relative to the slender body can be achieved, thereby permitting linear proportional control of the lateral force and moment.[15] Although many experimental studies have been conducted on this topic, there is still a lack of consensus among the experimental analysis of the pressure and PIV measurements for high-spatiotemporal-resolution flow fields.

To further improve the efficiency of plasma actuators, to narrow the gap with respect to actual engineering applications, and to identify the control mechanisms for forebody asymmetric vortices based on plasma actuation, this paper reports wind tunnel experiments conducted with an innovative EX-DBD actuation, which has a strong tendency to induce jet flow by increasing the electric field downstream of the ionic wind.[16–18] Through synchronous measurements of the pressure distribution and PIV flow visualization, the desired control effects of plasma actuation on boundary layer separation and the spatial topological structures of the asymmetric vortices are obtained, and the corresponding control mechanisms are identified. The present results can provide technical guidance for the control and reuse of forebody vortices.

2. Description of the experimental setup

Experiments were conducted in a low-speed closed-return wind tunnel of the Air Force Engineering University. The wind tunnel was 19.79 m long and 10.16 m wide. The test section was 3 m long and had a rectangular cross section that was 1.2 m wide and 1.0 m high (see Fig. 1(a)). The speed of the wind tunnel was adjustable in the range of $U_\infty = 5$–75 m/s with a turbulence level of $\varepsilon \leq 0.2\%$. The test section included three interchangeable glass windows that provided good access for optical diagnostics. Two transparent glass windows were installed on the left and right sides of the test section, and an optical glass window was installed on the upper side of the section for the PIV experiment.

The slender body model used in these experiments consisted of a circular cone and a cylindrical afterbody (see Fig. 1(b)), which were made of Bakelite materials and had a total length of $L = 500$ mm. The circular cone had a 10° semi-apex angle. The base diameter of the cylindrical afterbody was $D = 120$ mm. The angle of attack of the slender body model was set to $\alpha = 45°$, and the sideslip angle was fixed at zero. The free-stream velocity U_∞ was chosen at 10 m/s, which corresponded to a Reynolds number of 0.75×10^5 based on the model base diameter.

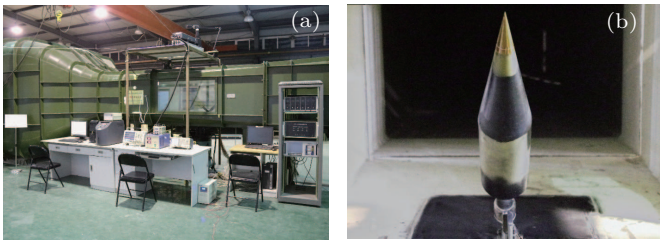


Fig. 1. (a) The experimental layout and (b) the slender body model in the wind tunnel.

Surface pressure measurements were performed to analyze the flow control performance. Four pressure measurement stations were mounted on the model at intervals of 20 mm along the middle axis. Twenty-four pressure transducers were circumferentially distributed at each station with azimuth angle intervals of $\Delta\theta = 15°$. The time-averaged pressure transducers used in these experiments were Model 9816 devices manufactured by the PSI Company, which recorded samples at a frequency of 100 Hz and had an accuracy rate below 0.1%. Continuous 10 s samples from the steady pressure transducers were recorded for analysis. The right side of the cone when facing the free stream is defined as the starboard side, and the left side from the same perspective is defined as the port side. The middle of the windward side is defined to be corresponding to an azimuth angle of $\theta = 0°$, and the counterclockwise direction is defined as the positive direction.

A two-dimensional PIV system was used to visualize the detailed structure of the flow field. The surface of the slender model was painted black to diminish laser reflection. The images were captured using a 2048×2048 pixel^2 CCD camera with a 100×80 mm^2 field of view. The frequency of image acquisition was 5 Hz. The Insight 3 G software package was used to process the recorded data. The final interrogation window size and overlap ratio used in the PIV cross correlation were 32×32 pixels^2 and 75%, respectively. To obtain tracer particles for PIV imaging, the whole test section of the wind tunnel was seeded with smoke particles in a mean diameter of 1 μm. The measurement position of the PIV system coincided with the location of the first pressure measurement station at the $1.25D$ cross section ($L = 150$ mm).

To ensure the repeatability of the pressure measurement results, pressure data were collected three consecutive times under each experimental condition, and the results of all three pressure measurements coincided. PIV measurements were collected for 10 s continuously for each case, with a time delay of 200 μs between consecutive images. Finally, the overall average pressure and PIV visualization results were calculated for the flow field analysis. To ensure the accuracy of the test

data, pressure and PIV data were not collected until the flow field had reached a stable pattern, 300 s after the working parameters had been changed, each time. The pressure and PIV results for the plasma-off mode were collected before and after plasma actuation under different working conditions. The experimental results show that the flow pattern for the plasma-off mode may differ under different working conditions due to changes in the external environment and the spatial instability of the asymmetric vortices caused by local microdisturbances around the tip of the slender model.[1–4] The purpose of applying the forebody vortex control technique was to transform the random flow into a controllable steady flow. Fortunately, for all wind tunnel tests in the same batch, the forebody vortex distribution of the flow field was essentially the same before and after the application of plasma actuation.

By analyzing the installation positions of the plasma actuators on the slender body model, it was found that the flow control effect was better when the DBD actuators were installed on the left and right sides of the cone head at $\theta = \pm 90^\circ$ in the circumferential direction, i.e., with the positions of the two actuators at the maximum circumferential separation on the surface of the cone. If the installation position of an actuator was to be changed relative to this configuration, the circumferential distance between the actuators would be shortened, which could easily result in a spark discharge at the front end of the exposed electrode due to the higher local electric potential. The high temperature generated by this spark discharge could easily burn through the dielectric layer of the actuator. The actuator configuration considered in this paper is a four-electrode actuator configuration that can produce EX-DBD output. Such an EX-DBD actuator is obtained by adding an exposed sliding electrode, which is connected to a positive dc high voltage, to a typical DBD actuator. The purpose of this approach is to enhance the potential difference in the negative half cycle of the ac voltage, to accelerate the movement speed of negative particles, and to generate a larger body force and electric wind.[9]

First, a pair of exposed strip electrodes were symmetrically placed on the slender forebody at circumferential angles of $\theta = +90^\circ$ and -90°. They shared a fan-shaped encapsulated electrode at the bottom of the insulating layer between the two exposed electrodes. Each exposed strip electrode was 70 mm long and 1 mm wide and was made of 0.3-mm-thick copper foil (see Fig. 2). Previous studies have found that the closer to the apex of the cone an actuator is, the better its flow control effect will be. However, if it is too close to the cone apex, the front end of the exposed electrode may be prone to spark discharge. Thus, the following two design principles were considered: the position of the actuator should be as close as possible to the cone apex, and spark discharge at the leading end of the actuator should be prevented. The front end of each exposed strip electrode in this experiment was 20 mm from the cone apex, similar to the configuration of the plasma actuators used in Refs. [12,15]. To further improve the flow control effect, an isosceles triangular sliding electrode made of 0.03-mm-thick copper foil was added to the upper surface of the insulating layer located between the two exposed strip electrodes. Both sides were 10 mm from the exposed strip electrode, enabling EX-DBD generation. The length of the two equal sides of the isosceles triangular electrode was approximately 30 mm, the length of the bottom side was approximately 15 mm, and the front end was 60 mm from the cone apex. The three corners of the isosceles triangular electrode were manually trimmed to form smooth circular chamfers to prevent spark discharge from this electrode.

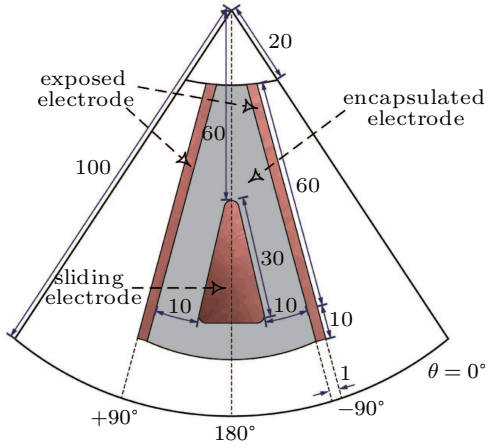


Fig. 2. EX-DBD plasma actuator on the slender forebody.

Three different modes of plasma actuation were tested to assess the effectiveness of forebody vortex control for the slender model. The typical DBD actuation mode, with the two long exposed strip electrodes connected to the ac power source and the triangular sliding electrode disconnected, was considered as the baseline for comparison. In the EX-DBD actuation mode, the two long exposed strip electrodes were connected to the ac power source, and the triangular sliding electrode was connected to a positive dc high voltage. The plasma-off mode corresponded to the case in which the plasma actuators were not activated.

A high-voltage sinusoidal ac wave source (model CTP-2000 K, Corona Laboratory) was used to generate basic DBD actuation, and the peak-to-peak voltage V_{AC} was set to 16 kV. The carrier frequency was in the range of $F = 6.5$–8.5 kHz. The encapsulated electrode was grounded. The pulse frequency f_p was varied from 50 Hz to 1000 Hz to study the dynamic interactions between the plasma actuation and the asymmetric flow. The duty ratio τ was varied from 10% to 100% to study the relationship between the pressure distribution and the lateral force at different duty ratios. A high-voltage dc power source together with the ac power source was

used to generate EX-DBD actuation. For this purpose, the dc power source was varied in a voltage range from −20 kV to +20 kV.

3. Analysis

3.1. Actuation optimization

To improve the control efficiency for asymmetric vortices, most previous studies have focused on optimizing the electrical parameters and geometric configuration of the plasma actuators, whereas there have been few studies on the control effect of changing the discharge regime of the plasma actuators. In this paper, a new four-electrode plasma actuator configuration, which makes the EX-DBD discharge, is adopted to enhance the induced body force and electric wind.

Based on previous experiments in a static atmosphere,[9] electrical parameters that provide effective flow control were selected (a pulse frequency of $f_p = 500$ Hz and a duty ratio of $\tau = 50\%$). The slender body model was tested at $\alpha = 45°$ and $U_\infty = 10$ m/s, with a Reynolds number of approximately 0.75×10^5. Other electrical parameters of the actuators were as follows: the ac peak-to-peak voltage V_{AC} was set to 16 kV, the carrier frequency was fixed at $F = 8.25$ kHz, and the dc high voltage was $V_{DC} = +6.2$ kV.

The pressure coefficient C_p is defined as follows:

$$C_p = \frac{P_{ni} - P_\infty}{P_o - P_\infty} = \frac{P_{ni} - P_\infty}{q_\infty}, \tag{1}$$

where P_{ni} is the static pressure measured at the i-th pressure measurement hole on the n-th cross section; P_∞ is the free-stream static pressure; and P_o and q_∞ are the total pressure and the free-stream dynamic pressure, respectively, at the reference point in the wind tunnel. Here, the reference point was selected to lie at the entrance to the wind tunnel test section.

Figure 3 shows the time-averaged pressure distributions at the first cross section of $1.25D$. When the plasma actuator is powered off, the right suction peak reaches the higher extreme value of $C_p = -0.538$ at $\theta = 270°$, and the left suction peak reaches the lower extreme value of $C_p = -0.045$ at $\theta = 90°$. This result indicates that the separation vortex on the right side is closer to the model surface than the separation vortex on the left side. Thus, the flow field is an asymmetric pattern. When the EX-DBD actuation is turned on, the suction peak on the left side rises. The flow field tends to be approximately symmetrical.

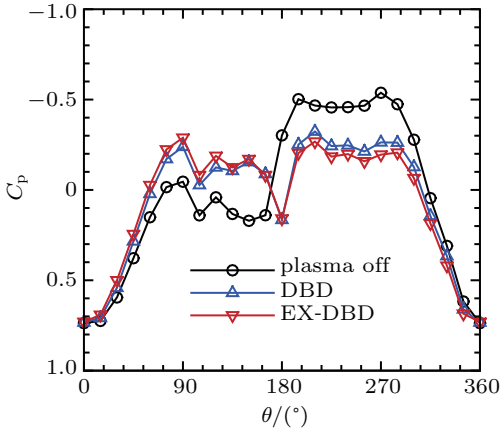


Fig. 3. Comparison of the pressure distributions under DBD and EX-DBD actuation.

In Fig. 4, the axial-vorticity contours represent the ensemble averaged vorticity calculated by axial-velocity distribution. Here the axial-vorticity intensity is defined as

$$\omega_z = \nabla \times u, \tag{2}$$

otherwise known as the curl of the velocity field. The dark blue represents the positive clockwise vorticity and the dark red represents the negative anti-clockwise vorticity. As seen from the velocity and vorticity contours in Fig. 4, after the application of EX-DBD actuation, the core position of the vortex on the right side moved from $y = 62.65$ mm to $y = 35.15$ mm, closer to the model surface than the core position of the vortex on the left side. The spatial positions of the vortex cores with DBD actuation were similar to those with EX-DBD actuation, but the suction peak on the left side under DBD actuation ($C_p = -0.250$) at $\theta = 90°$ was slightly lower than that under EX-DBD actuation ($C_p = -0.289$).

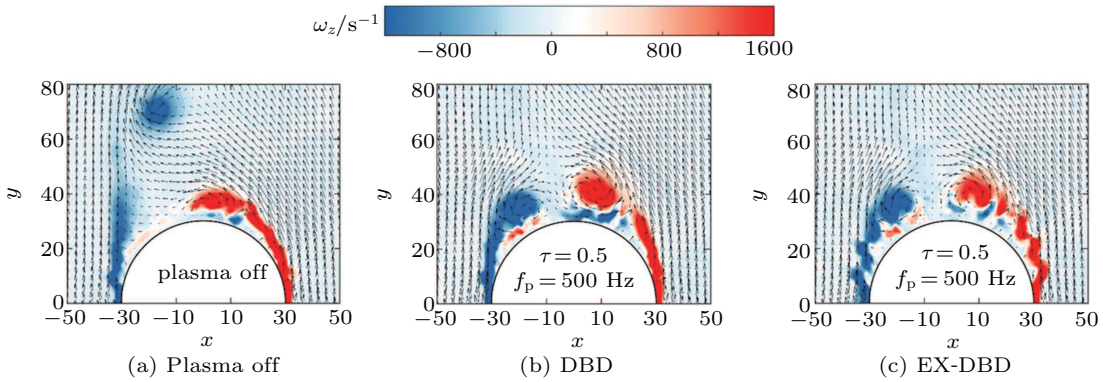


Fig. 4. Time-averaged axial-vorticity contours overlaid with streamlines for DBD and EX-DBD actuations.

To analyze the flow control effect for different types of plasma actuation, a sectional lateral force coefficient C_{Yd}, which is a nondimensional parameter that reflects the sectional lateral force at a measured pressure station with respect to the free stream, is defined as

$$C_{\mathrm{Yd}} = \frac{Y_{dn}}{dq_\infty} = \frac{\sum_{i=1}^{k}(P_{ni} - P_\infty)\sin\theta_i \cdot \Delta\theta \cdot \pi}{360 q_\infty}. \tag{3}$$

The sectional side force Y_{dn} at the n-th cross section can be calculated by integrating the circumferential pressure distributions.[10,15] Y_{dn} is normalized with respect to the free-stream dynamic pressure q_∞ and the local cone diameter d to obtain the sectional side force coefficient C_{Yd}. The sign of this force is positive when it is pointing toward the starboard side of the cone. The plasma actuators circumferentially generate plasma discharge on the slender forebody surface. Therefore, the characteristic length d ($= 55\ \mathrm{mm} \times \sin 10^\circ \times 2 = 19.1\ \mathrm{mm}$) is the local diameter of the cone at the center of the plasma actuators. Here θ_i is the azimuth angle of the i-th pressure measurement hole in the model, and $\Delta\theta$ is the circumferential angular interval between the pressure measurement holes at each pressure measuring station. In this experiment, there were four stations on the slender model, and each station included 24 evenly spaced pressure measurement holes. Therefore, the circumferential angular interval between measurement holes was $\Delta\theta = 15^\circ$.

To facilitate a comparative analysis of the pressure measurement and PIV results, the sectional lateral force coefficient at the first cross section of $1.25D$ is analyzed here. When plasma actuation was turned off, the sectional lateral force coefficient was $C_{\mathrm{Yd}} = 0.470$. After the application of DBD actuation, C_{Yd} was 0.123, and after the application of EX-DBD actuation, the sectional lateral force coefficient was $C_{\mathrm{Yd}} = 0.027$. These results correspond to decreases in the sectional lateral force coefficient of 73.8% for DBD actuation and 94.3% for EX-DBD actuation. Thus, the lateral force can be effectively reduced by applying both of plasma actuations.

Through a comprehensive analysis of the pressure distribution, PIV and sectional lateral force coefficient results, it is found that EX-DBD for forebody vortex control has a better capacity than DBD. The negative space charge created by a single DBD during the negative-going cycle is more accelerated in the case of EX-DBD actuation, resulting in a faster time-averaged velocity and an enhanced body force.[18] Under the condition of no incoming flow, EX-DBD will intensify the movement of the original charged ions from DBD and result in charge accumulation on the surfaces of the actuators, thereby generating a secondary electric field that will weaken the external electric field and reduce the size of the overall electric field in the discharge area, consequently reducing the flow control efficiency. However, in these wind tunnel experiments, EX-DBD demonstrated a superior flow control capacity because the charged ions on the actuator surfaces could be blown away by the incoming flow. This finding also verifies the results reported in Ref. [19].

In contrast to the plasma actuator configuration used in this paper, the control strategies applied in Refs. [8,12] involve single-sided pulsed duty ratio or double-sided duty cycle modulation plasma actuation. These control strategies are suitable for situations in which the direction and magnitude of the lateral force are known. However, the flow field pattern of the experimental model is not known, such control strategies are not optimal. Instead, this paper focuses on a control scheme based on synchronous actuation on both sides of the slender body, which eliminates the need for auxiliary duty cycle control equipment, reduces the complexity of the power supply system, and simplifies the control procedure for asymmetric vortices. In practical applications, if phantom yaw occurs or random lateral forces are detected, the plasma actuators on both sides of the aircraft forebody simply need be turned on simultaneously, without considering the direction and strength of the lateral force, allow the spatial distribution of the asymmetric vortices alone.

4. Linear proportional control of sectional lateral force

To facilitate engineering applications and the automatic pilot function for advanced aircraft, the ultimate goal of forebody vortex control is to achieve the proportional control and closed-loop control of lateral forces. In this section, the influences of the pulsed duty ratios of DBD and EX-DBD actuations on the pressure distribution and lateral force are studied. Notably, our research group is currently studying a miniaturized plasma closed-loop control system. Ideally, this system could be applied for the control of the asymmetric vortices around slender bodies at high angles of attack, flight attitude control for unmanned aerial vehicles (UAVs), deicing/anti-icing, drag reduction, etc.

To realize proportional control of the pressure distribution and lateral forces, methods such as adjusting the pulsed duty ratio of plasma actuation are generally employed at present. Future research should focus on simplifying the applied control scheme, improving control efficiency and reducing energy consumption. Figure 5 illustrates the pressure distribution results obtained when EX-DBD actuation was applied with different pulsed duty ratios. The plasma-off mode represents the case in which the plasma actuators were turned off, and $\tau = 100\%$ represents continuous actuation. When the plasma actuators were not turned on, the suction peak on the right side was higher than that on the left. As the duty ratio was increased from 10% to 90%, the suction peak on the right side

gradually declined, and the suction peak on the left side gradually increased in magnitude and peaked at $\tau = 70\%$. As the duty ratio was further increased, the asymmetric flow first became symmetrical and then evolved into a flow pattern with the opposite asymmetry. Correspondingly, the side force first decreased to zero and then began to increase in the opposite direction. When the duty ratio reached $\tau = 100\%$, the control effect was not improved and, in fact, was worse than that at $\tau = 30\%$. This result is also consistent with the conclusions of Ref. [12].

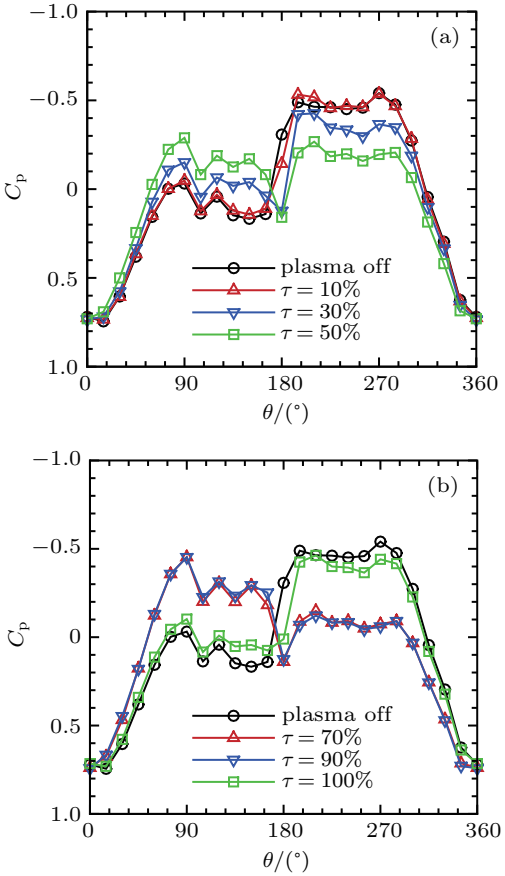


Fig. 5. Pressure distributions under EX-DBD actuation with different duty ratios.

Unsteady pulsed plasma actuation can generate large-scale vortex structures in the boundary layer, which can entrain the kinetic energy from the external flow into the boundary layer and change the position of the boundary layer transition and the spatial distribution of the vortex structure, thereby achieving a flow control effect. When pulsed plasma actuation is turned on, the induced flow field takes shape and begins to stabilize within a short period of time.[19] By increasing the duty ratio of plasma actuation, the intensity of the induced starting vortex can be slightly improved, whereas there will not be a great impact on the induced body force and momentum. Although the input energy can be continuously increased in the case of steady plasma actuation, it is not conducive to the formation of large-scale vortex structures. Accordingly, pulsed plasma actuation not only can provide a better control effect than steady actuation but also can save more energy.

Figure 6 compares the performances of DBD and EX-DBD actuations on the sectional lateral forces based on the measured pressure. When the duty ratio was less than 30%, the control effects of both plasma actuation modes on the sectional lateral forces were basically the same. When plasma actuation was turned off, the sectional lateral force coefficient was $C_{Yd} = 0.470$; the control effect of DBD reached a minimum value ($C_{Yd} = -0.061$) at $\tau = 70\%$. As the duty ratio was further increased, the effect of forebody vortex control declined due to the recovery of the sectional lateral force. By contrast, the sectional lateral force coefficient under EX-DBD was basically stable at $\tau = 70\%$ and reached its maximum value ($C_{Yd} = -0.193$) at $\tau = 90\%$. Therefore, EX-DBD actuation increased the maximum sectional lateral force coefficient by 24.9% compared to that under DBD actuation in this investigation of different pulsed duty ratios. At $\tau = 100\%$, the sectional lateral forces under DBD and EX-DBD actuations were nearly the same, suggesting that the difference in the control effect of steady discharge between different plasma actuator configurations or plasma discharge regimes is very small.

From the relationship between the sectional lateral force and the pulsed duty ratio depicted in Fig. 6, the sectional lateral force monotonically decreases with increasing duty ratio, thus the linear control of the lateral force on the slender body can be achieved by modifying the duty ratio. It can also be inferred that to decrease the sectional lateral force on the slender body to zero, a pulsed actuation with a duty ratio of 63.5% would be needed for DBD, in comparison with a duty ratio of only 52.8% for EX-DBD, representing an energy saving of 20.3%. Furthermore, EX-DBD actuation not only can achieve lateral force control with less energy consumption than DBD actuation but also can reverse the direction of the lateral force. Hence, EX-DBD actuators are found to be more capable of controlling forebody asymmetric vortices than DBD actuators and to enable linear control of the lateral forces on a slender body by varying the duty ratio. However, in this experiment, there was no standard linear proportional control relationship between the DBD duty ratio and the sectional lateral force. When the duty ratio was greater than 70%, the control effect weakened, in contrast to the conclusion in Ref. [12]. The reason for this discrepancy may be that wind tunnels can differ widely in their noise levels, resulting in different separation phenomena for the boundary layers around slender models. In addition, the forebody vortices are very sensitive to microdisturbances near the tip of a slender model. The microdisturbances generated by mismachining tolerances, which are called background disturbances, will also result in different lateral forces. In future research, it is anticipated that a linear proportional control strategy will be found that is suitable for

experimental models of similar sizes and configurations.

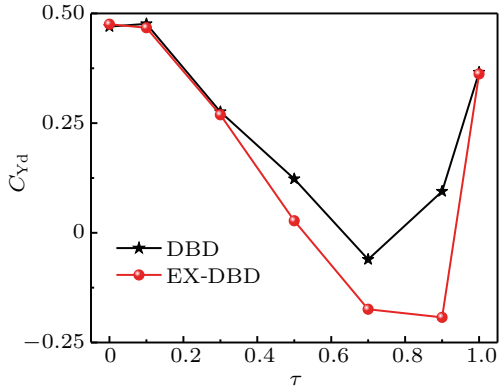


Fig. 6. Comparison of the sectional lateral forces under DBD and EX-DBD actuations with different duty ratios.

5. Frequency coupling mechanism

The pulsed duty ratio and pulse frequency are two key factors influencing plasma flow control. The pulsed duty ratio mainly affects the energy intensity of the plasma-induced jet, namely, the amount of momentum injected into the boundary layer or flow field. However, with a reasonably selected pulse frequency, a mutual coupling effect between the plasma actuation frequency and the natural frequency of the forebody vortex system in the flow field may be achieved, leading to a phenomenon similar to frequency resonance, which is expected to further enhance the flow control effect.

Figure 7 displays an analysis of the flow control effects of EX-DBD actuation at different pulse frequencies. When plasma actuation was turned off, the suction peak on the right side was higher than that on the left, and the suction peak on the left side ($C_p = -0.029$) appeared at $\theta = 75°$. When EX-DBD actuation was turned on, the suction peak on the left side gradually increased in magnitude with increasing pulse frequency and reached its maximum ($C_p = -0.302$, $\theta = 90°$) at $f_p = 200$. At this point, the difference between the heights of the suction peaks on the left and right sides had decreased, indicating that the forebody flow field had gradually changed from a topological structure with asymmetric vortices to symmetric vortices, and the magnitude of the sectional lateral force had decreased accordingly. As the pulse frequency was further increased to $f_p = 500$ Hz, the pressure distribution curve changed very little, and the flow control effect slightly weakened. When the pulse frequency was further increased to 1000 Hz, the suction peak on the left side decreased sharply, and the control effect was even worse than that for the frequency 50 Hz. Additionally, as illustrated in Fig. 7, after plasma actuation was applied, the position of the extreme value of the suction peak on the left side changed from $\theta = 75°$ to $\theta = 90°$, indicating that the flow separation in the leeward region of the slender body was effectively suppressed.

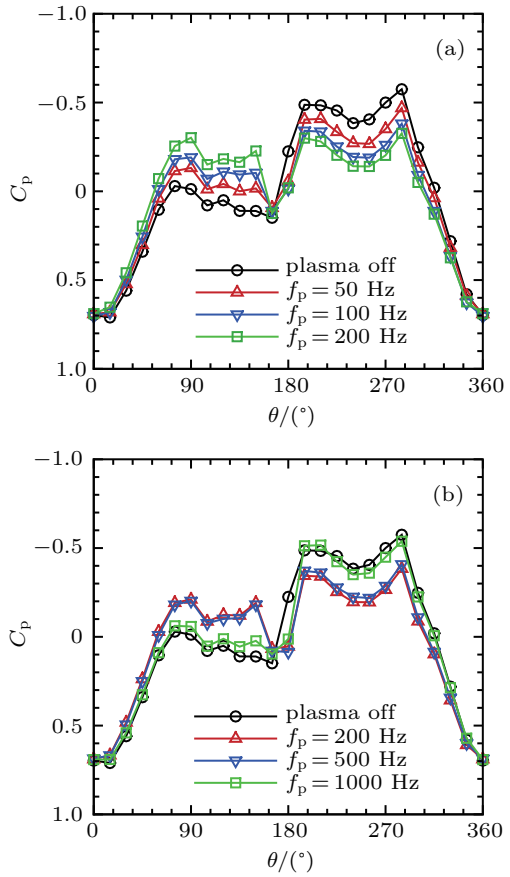


Fig. 7. Pressure distributions under EX-DBD actuation with different pulse frequencies.

Figure 8 presents a visualization of the PIV flow field to illustrate the spatial distribution of the asymmetric vortices at the 1.25D cross section. When the plasma actuators were turned off, the blue vortex on the left side was far away from the model surface (higher-position vortex), and the red vortex on the right side was close to the model surface (lower-position vortex), forming an asymmetric spatial distribution. When EX-DBD plasma actuation was turned on, the higher-position vortex on the left side approached the model surface, but the lower-position vortex on the right side did not shift considerably, and the flow field distribution became approximately symmetric. However, when the pulse frequency was increased to $f_p = 200$ Hz, the lower-position vortex on the right side began to rise away from the model surface. As the pulse frequency was further increased, the control effect gradually weakened, and the flow field returned to its previous state without plasma actuation. This is consistent with the results of pressure distributions in Fig. 7.

The phase-locked PIV results reported in Ref. [20] indicate that a vortex structure, of which the size increases as the pulse frequency decreases, is shed from the shear layer with each plasma actuation pulse. A large-scale vortex structure generated at a low pulse frequency can affect the flow field by means of vortex entrainment, draw kinetic energy from the external flow into the boundary layer and affect the po-

sition of the boundary layer transition. A small-scale vortex structure generated at a high pulse frequency can promote a turbulent transition, and both the transition and reattachment points will move upstream with increasing pulse frequency or input voltage.[21] It is surmised that there exists a certain natural frequency in every forebody flow system. When the pulse frequency is approaching to this natural frequency, the amplitude of the spatial variation of the asymmetric vortices will be abruptly augmented, and the control effect of plasma actuation will be significantly improved, through a phenomenon similar to frequency resonance. However, changing the experimental conditions may alter the natural frequency of the flow system.

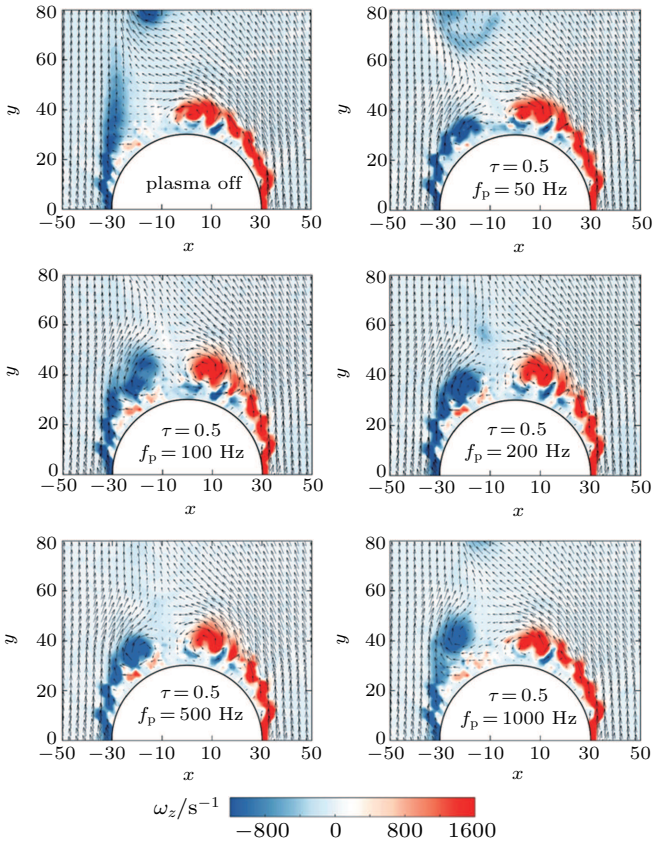


Fig. 8. Time-averaged axial-vorticity contours overlaid with streamlines for EX-DBD actuation with different pulse frequencies.

Figure 9 presents a comparative analysis of the sectional lateral forces observed under DBD and EX-DBD actuations with different pulse frequencies. When the plasma actuators were turned off, the flow field was in an asymmetric state with a large sectional lateral force ($C_{Yd} = 0.532$). The higher-position vortex appearing on the left had only a small total pressure loss of the ambient fluid near the model surface, corresponding to a lower suction peak on the left. By contrast, the lower-position vortex appearing on the right had a large total pressure loss of the ambient fluid near the model surface, corresponding to a higher suction peak on the right. Thus, the slender body model was subjected to a sectional lateral force toward the starboard side. When pulsed plasma actuation was turned on, the sectional lateral force decreased. The control effects of DBD and EX-DBD under pulsed actuation at $f_p = 50$ Hz were not different. As the pulse frequency was increased, the sectional lateral force in both the cases reached its minimum value ($C_{Yd} = 0.021$ for DBD and $C_{Yd} = -0.027$ for EX-DBD) at $f_p = 200$ Hz. Under EX-DBD actuation, the maximum sectional lateral force coefficient was increased by 8.6% compared with that under DBD actuation. Thus, after the plasma actuators were turned on, the peak values of the suction peaks on both sides tended to be similar (Fig. 7), indicating that the original asymmetric vortices had become basically symmetrical (Fig. 8), and the sectional lateral force was significantly suppressed. As the pulse frequency was further increased, the sectional lateral force increased again, indicating that the control of the asymmetric flow field was gradually becoming ineffective. When the pulse frequency was greater than 800 Hz, the lateral force control effect of EX-DBD actuation decreased faster than that of DBD actuation.

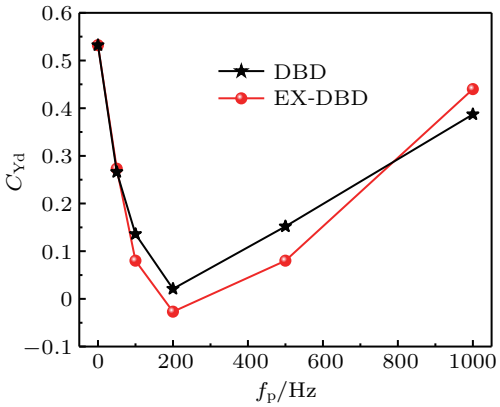


Fig. 9. Comparison of the sectional lateral forces under DBD and EX-DBD actuations with different pulse frequencies.

In Ref. [13], the control effect of plasma actuation for asymmetric vortices was optimal when the normalized reduced frequency reached $f^+ = 1$. However, for the experimental model used in the wind tunnel experiments reported in this paper, the optimal pulse frequency for asymmetric vortex control was $f_p = 200$ Hz, corresponding to a normalized reduced frequency of $f^+ = 2\pi f_p d/U_\infty = 2.39$. These different optimal pulse frequencies may be due to the different experimental models and experimental environments considered. However, it has been proven that an optimal pulse frequency does exist in many studies on forebody vortex control by means of plasma actuation. Therefore, reasonable selection of the pulse frequency is critical because an overly high frequency will waste energy, while an overly low frequency will not achieve the best control effect.

6. Conclusions

We have reported wind tunnel experiments involving forebody asymmetric flow control for a slender body at high

angles of attack conducted using a new extended dielectric barrier discharge (EX-DBD) actuator, which has a stronger capacity to induce electric wind than a DBD actuator. A control scheme based on synchronous EX-DBD actuation on both sides of the slender body has been investigated, which eliminates the need for auxiliary double-sided duty cycle control equipment and reduces the complexity of the power supply system. The maximum sectional lateral force coefficients under EX-DBD actuation are increased by 24.9% and 8.6% compared to those under DBD actuation in analysis of different pulsed duty ratios and pulse frequencies, respectively. EX-DBD actuators are found to be more capable of controlling forebody asymmetric vortices than DBD actuators, and linear control of the lateral force on the slender body can be achieved by modifying the duty ratio. Under the present experimental conditions, there exists an optimal normalized reduced frequency ($f^+ = 2\pi f_p d/U_\infty = 2.39$) for asymmetric vortex control. Therefore, reasonable selection of the pulse frequency is critical because an overly high frequency will waste energy, while an overly low frequency will not achieve the best control effect. Notably, most related studies to date have been based on experiments, and there is still a lack of numerical simulations of the dynamic process of plasma actuation control for asymmetric vortices. In the future, it will be necessary to incorporate simulation methods into further investigations of the control mechanism.

References

[1] Williams D R 1997 *AIAA* (*A review of forebody vortex control scenarios* in *28th Fluid Dynamics Conference*, 29 June–2 July 1997) p. 29
[2] Bridges D H 2010 *Prog. Aerosp. Sci.* **46** 62
[3] Ericsson L E 1992 *J. Aircraft* **29** 1086
[4] Wang Q T, Cheng K M, Gu Y S and Li Z Q 2018 *Phys. Fluids* **30** 024102
[5] Zhai J, Zhang W W and Wang H L 2017 *Acta Aerodynamica Sin.* **35** 354 (in Chinese)
[6] Fagley C, Porter C and McLaughlin T 2014 *AIAA J.* **52** 2891
[7] Maslov A A, Zanin B Y and Sidorenko A A 2004 *AIAA* 2004 843 (42nd AIAA Aerospace Sciences Meeting and Exhibit, 5–8 January 2004 Reno, Nevada)
[8] Wang J L, Li H X, Liu F, Luo S J 2010 *AIAA* 2010 1087 (48th AIAA Aerospace Sciences Meeting Including the New Horizons Forum and Aerospace Exposition, 4–7 January 2010 Orlando, Florida)
[9] Zheng B R, Ke X Z, Ge C, Zhu Y F, Wu Y, Liu F and Luo S J 2020 *AIAA J.* **58** 733
[10] Zheng B R, Gao C, Li Y B, Feng L and Luo S J 2013 *Plasma Sci. Technol.* **15** 350
[11] Long Y X, Li H X, Meng X S and Hu H Y 2018 *Appl. Phys. Lett.* **112** 014101
[12] Liu F, Luo S J, Gao C, Meng X S, Hao J N, Wang J L and Zhao Z J 2008 *AIAA J.* **46** 2969
[13] Zheng B R, Gao C, Li Y B, Feng L and Luo S J 2012 *Plasma Sci. Technol.* **14** 58
[14] Lombardi A J, Bowles P O and Corke T C 2013 *AIAA J.* **51** 1130
[15] Meng X S, Long Y X, Wang J L, Liu F and Luo S J 2018 *Phys. Fluids* **30** 024101
[16] Zheng B R, Xue M and Ge C 2020 *Chin. Phys. B* **29** 024704
[17] Michael J J and David B G 2017 *Plasma Sources Sci. Technol.* **26** 103002
[18] Benard N and Moreau E 2014 *Exp. Fluids* **55** 1846
[19] Zheng B R, Xue M, Ke X Z, Ge C, Wang Y S, Liu F and Luo S J 2019 *AIAA J.* **57** 467
[20] Sekimoto S, Nonomura T and Fujii K *AIAA J.* **55** 1385
[21] Vukasinovic B and Glezer A 2006 *AIAA* 2016 3227 (36th AIAA Fluid Dynamics Conference and Exhibit, 5–8 June 2006 San Francisco, California)